Engineering Failure Analysis 105 (2019) 1006–1017

Contents lists available at ScienceDirect

Engineering Failure Analysis

journal homepage: www.elsevier.com/locate/engfailanal

Reflectance Transformation Imaging as a tool for engineering failure analysis

H.E. Coules[a,*], P.J. Orrock[a], C.E. Seow[a,b]

[a] Department of Mechanical Engineering, University of Bristol, Bristol, UK
[b] National Structural Integrity Research Centre, TWI ltd., Great Abington, Cambridgeshire, UK

ARTICLE INFO

Keywords:
Fractography
Reflectance Transformation Imaging
Photogrammetry
Photometric stereo

ABSTRACT

Reflectance Transformation Imaging (RTI) is a technique which can be used to record the surface appearance of objects. It can capture a surface's interaction with incident light from different directions and it enables estimation of the surface normal vector. 3D surface profile information can be estimated from RTI datasets using photometric stereo methods. RTI currently has applications in archaeometry and cultural heritage studies but here we discuss the use of RTI in an engineering context: as a tool for failure analysis and particularly for examining failure surfaces in structural materials and components. We demonstrate that RTI can be a practical and low-cost technique for failure analysis, complementing other surface analysis and 3D scanning methods.

1. Introduction

1.1. Failure analysis and RTI

Macroscopic optical examination is a key step in any failure analysis of a broken structural component or material test specimen [1]. Optical examination of the failure surface is fast and cheap. In most cases it allows the analyst to establish the basic mechanism of failure from distinctive failure surface characteristics without resorting to higher-resolution techniques such as electron microscopy [2]. If the purpose of the investigation is to inform design or assign liability then a simple statement of the failure mechanism may be a sufficient result. In more detailed studies macroscopic examination provides a useful starting-point for any subsequent investigation. For example, to determine the crack growth rate in a fatigue fracture via SEM analysis, the fatigue crack surface must first be identified visually.

Surfaces formed by fracture, tearing, fatigue, corrosion and creep rupture are typically non-smooth, coloured and anisotropically reflective. While performing an initial examination of a failure surface, an analyst relies on their own visual perception and uses prior experience of examining similar surfaces to determine the mechanism of failure. One aspect of our visual perception is stereopsis: we appreciate 3D shape by using our binocular vision as well as monocular visual indications including motion parallax and perspective. However, non-topological information including angle- and colour-dependent reflectance is also vital for our perception of surfaces. When performing an initial examination of a failed component, the analyst unconsciously synthesises these different aspects of their visual perception: multiple visual cues are used to differentiate between a failure surface formed by cleavage fracture and one formed by ductile tearing, for example.

Reflectance Transformation Imaging (RTI) is an imaging technique used to capture the surface appearance of objects. A set of

* Corresponding author.
E-mail address: harry.coules@bristol.ac.uk (H.E. Coules).

https://doi.org/10.1016/j.engfailanal.2019.07.037
Received 2 April 2019; Received in revised form 11 July 2019; Accepted 14 July 2019
Available online 23 July 2019

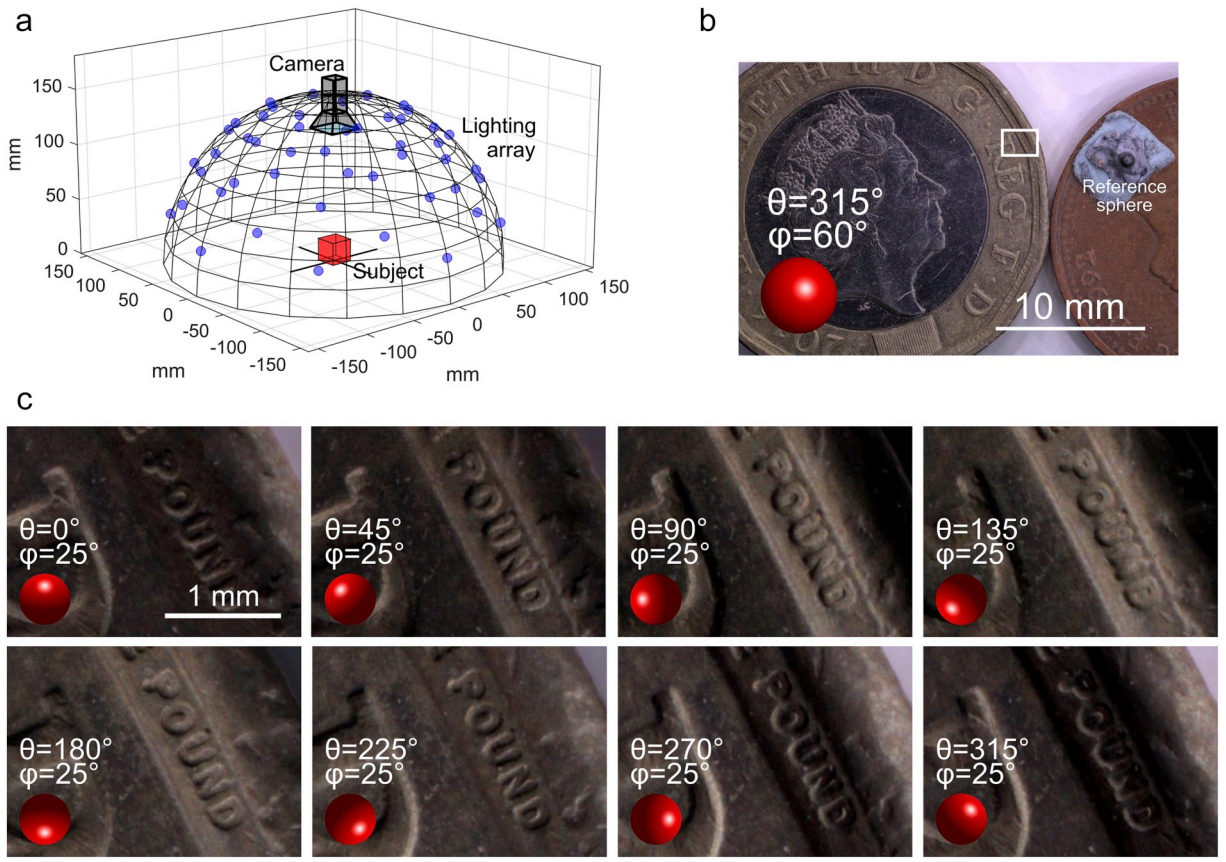

Fig. 1. Basic principle of RTI. a.) Image capture arrangement, b.) Single image of UK £1 and 1p coins with 1 mm dia. Reference sphere. c.) Close-ups of the £1 rim micro-inscription of the under illumination from eight different specified directions (azimuth θ, elevation φ), created after capture by virtual re-lighting of the image using an HSH texture model.

images of the subject are taken using a fixed viewpoint and with a fixed optical system, but with illumination from a light source at a different position in each image (see Fig. 1). The captured images are in pixel register but show the subject under different lighting conditions. In RTI, these images are used to create a texture map in which the red, green and blue values of each pixel are given as a continuous function of the direction vector of the incident light. For example, in the Polynomial Texture Mapping (PTM) scheme developed by Malzbender et al., a pixel's luminance is modelled as a biquadratic function of the projection of the lighting vector onto the image plane [3,4]. In the similar Hemispherical Harmonics (HSH) scheme proposed by Gautron et al. [5] and implemented by Wang et al. [6], the relationship between the lighting vector and the pixel's luminance is modelled using a hemispherical basis [7]. Finally, Pitard et al. have recently proposed a modal basis for describing this relationship, termed Discrete Modal Decomposition (DMD) [8].

After a set of RTI images of a subject have been taken, PTM, HSH or DMD basis coefficients for each pixel are calculated by least-squares fitting of the texture model to the image set. Using this model which relates the lighting direction to the appearance of the subject, subtle surface features can be appreciated better than with a single image [9]. Surface features can cause differences in surface specularity, colour variations, and surface topography – all of which are affected by the viewing angle. In a physical specimen, topography is unconsciously inferred by the viewer from point-to-point differences in luminance variation and from shadowing.

So far, the development of RTI has focussed largely on cultural heritage applications such as the examination and digitisation of archaeological specimens and artistic works [10–14]. The use of RTI on specimens from the biological sciences has also been reported, notably fossils [3]. So far, the only engineering application of RTI is for characterisation of surface finish, as reported by Pitard and co-workers [15,16]. In this article, we examine the use of RTI for failure analysis and show that it can be used to aid the macroscopic observation of topographical features on failure surfaces in engineering and materials science.

1.2. RTI equipment

Image capture for RTI is performed using a fixed camera and either a lighting array or a single light which can be moved around the subject in-between shots. Synchronisation between the lights and the camera are required to ensure that in each image, the scene is lit from a different angle. The number of lighting angles required to minimise error depends on the basis used for lighting

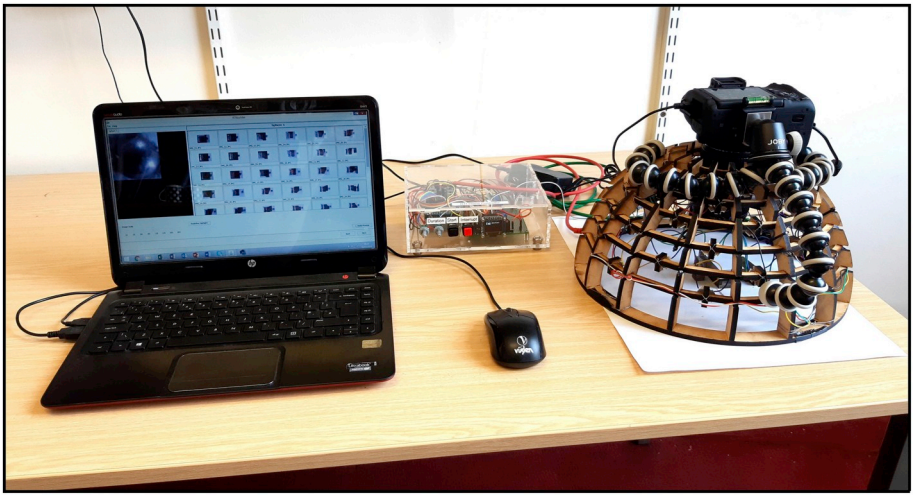

Fig. 2. Simple RTI imaging setup comprising an SLR camera, hemispherical lighting array, lighting array controller and laptop computer. The software visible is RTIBuilder by Cultural Heritage Imaging [18].

interpolation [13,17].

We constructed the simple macrophotography RTI setup shown in Fig. 2. It has four main parts: a camera, a dome-shaped LED light array, a lighting array controller and a laptop for saving and post-processing the RTI images. The camera is a 24 Megapixel Canon EOS 760D Digital SLR mounted pointing vertically downward at the apex of the lighting array dome. Three different lens arrangements were used for the examples shown in this paper: a Canon EF 50 mm f/2.5 macro lens, the same lens with a 36 mm extension tube, and a reversed Canon EF 24 mm f/2.8 IS USM lens with a 36 mm extension tube. The lighting dome is hemispherical with a radius of 150 mm at the light positions. 48 white Cree XLamp XP-E2 High Power LEDs (Cree LED components, Durham, NC, USA) with a colour temperature of 4000 K are positioned to achieve equal-area spacing over the region of the hemisphere between 15° and 65° elevation [10]. The lighting array is controlled by an Arduino Mega microcontroller, programmed to light the LEDs in a predetermined sequence for a duration set by the user. The lighting array controller also uses an infrared LED to activate the camera's remote trigger. The laptop controls the camera's capture setting remotely via Canon's EOS Utility v3.10.0 software. The popular RTIBuilder v2.0.2 [18] and RTIViewer v1.1.0 [19] packages (Cultural Heritage Imaging, San Francisco, CA, USA) were used for processing of the RTI images, and custom code was written in MATLAB script (The Mathworks inc., Natick, USA) for 3D shape reconstruction.

The direction of incident lighting in each RTI image was determined using the specular highlighting method described by Mudge et al. [13]. Reference spheres of 0.5 mm and 1 mm diameter, used for determining the incident lighting vectors via the highlight method, were obtained from the tips of ballpoint pens. They were attached to small pieces of putty for ease of handling and were included in the frame of all captured images, as shown in Fig. 1b.

2. Use of RTI in failure analysis

2.1. Viewing surfaces with a different lighting vector post-capture

Regardless of which modelling scheme is used for representing the image's dependence on lighting direction, the result is a texture map that can simulate the subject's appearance under lighting from any direction, or combination of directions - a process termed ‘virtual relighting’ (see Fig. 1c). Just as one might turn an object over against the sunlight to better view its surface features, virtual relighting allows a user to appreciate of the appearance of the subject's surface more fully than from a single image with a single lighting condition. RTI viewing programs (such as Cultural Heritage Imaging's RTIViewer [19]) allow the lighting angle to be manipulated in real time by the user. Virtual relighting provides an opportunity to find and use lighting conditions that are favourable for discerning the features of interest for each individual specimen, and to do so after capture.

An example of relighting a failed component is shown in Fig. 3. The failed part is a ball-ended screw which locates in a socket to secure one end of a gas spring (Fig. 3a). The gas spring held open the wafer loading lid of an industrial semiconductor manufacturing tool. The part failed in shear at the thread, likely due to an operator error eg. the loading lid being closed on an object. Few features of the fracture surface can be seen under poor illumination conditions in Fig. 3b. However, a shallower lighting angle (raked lighting) can be effective for showing the low-relief features which occur on failure surfaces [20]. Virtual relighting of this scene with lighting from the side (Fig. 3c) and with deeply-raked lighting (Fig. 3d) emphasises the fracture surface relief and makes it possible to determine the mode of failure and direction of shear.

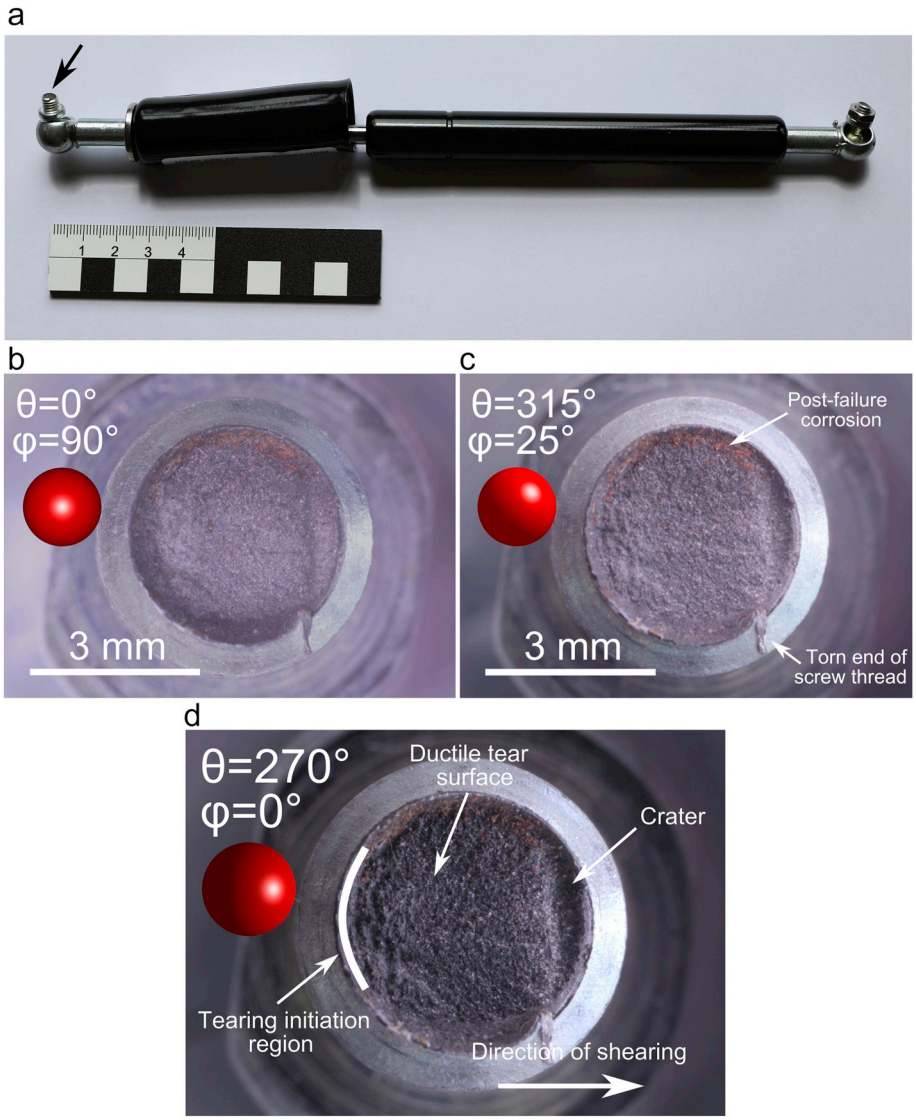

Fig. 3. Gas spring ball joint sheared at a threaded connection. a.) Location of the fracture surface on the gas spring assembly. b.) Fracture surface under a poor illumination condition (12-o'clock position, as with a ring light), showing only basic features. c.) Improved view with lighting from the top-right. d.) Fracture surface under strongly-raked lighting, emphasising surface relief.

2.2. Specular enhancement

Malzbender et al. have outlined methods of RTI for contrast enhancement [4]. One such method is specular enhancement: by using the surface normal vector in a lighting equation, it is possible to produce a synthetic image of the subject in which the specularity is artificially enhanced. For example, in the Phong lighting model, the luminance I of a point is given by [21]:

$$I = k_a i_a + \sum_{m=1}^{M} [(\hat{l}_m \cdot \hat{n}) k_d i_{dm} + (\hat{h}_m \cdot \hat{n})^{\alpha} k_s i_{sm}] \tag{1}$$

where $\hat{n}$ is a unit vector representing the surface normal. For each of M light sources, the direction of the light source from the surface point is $\hat{l}_m$ and $\hat{h}_m$ is a unit vector bisecting the angle between the light source and the viewer, while i_{dm} and i_{sm} are the light source's diffuse and specular intensities. The ambient light intensity is i_a. k_a, k_d and k_s are the ambient, diffuse and specular reflection constants of the surface and α is its shininess. Using the known $\hat{n}$ for each pixel, a simulated image with increased specularity can be produced by applying a pixel-wise proportionate increase in k_s.

In failure analysis, specular enhancement can be used to improve the visibility of topographical features on failure surfaces. Fig. 4 shows the fracture surface of a high-strength steel compression spring from an automotive suspension which failed in-service. The failure occurred close to the end of the spring where the wire diameter was approximately 11 mm. The failure surface has a typical

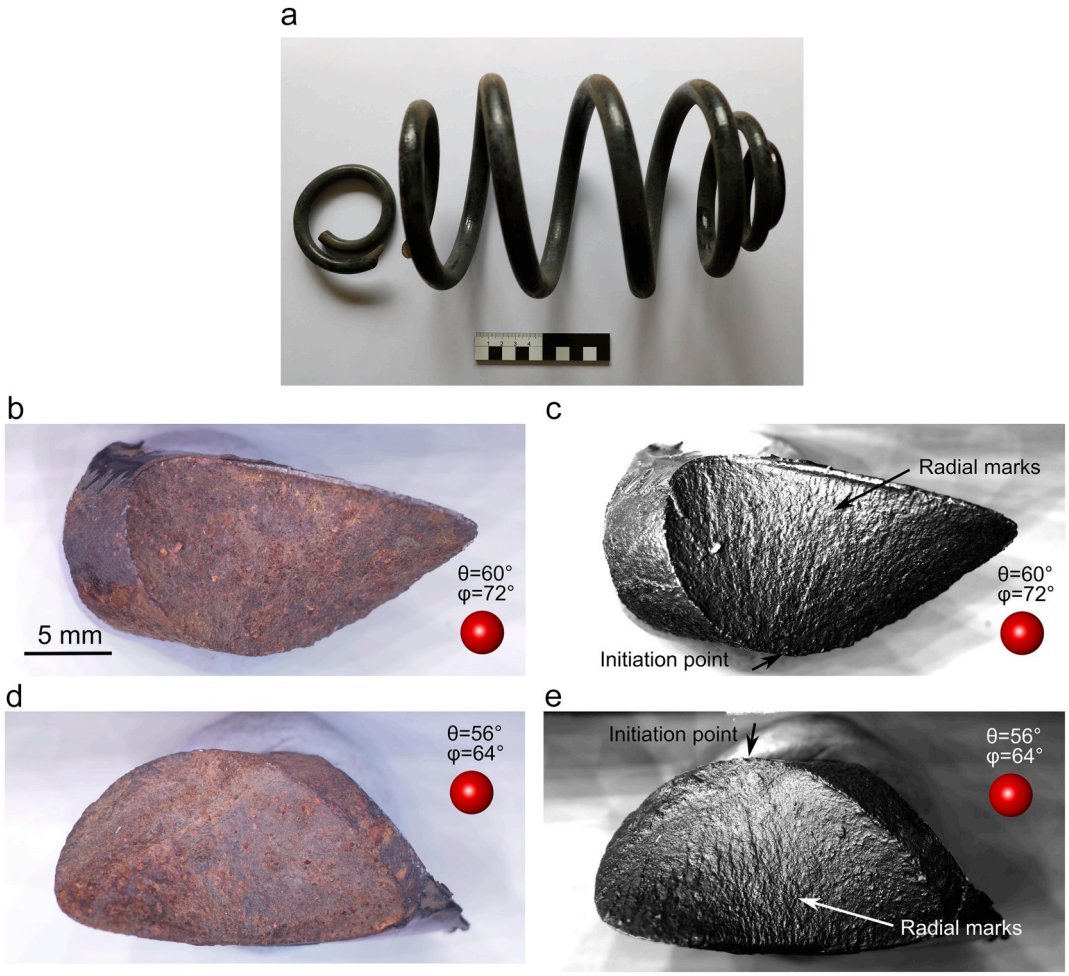

Fig. 4. Oxidised fracture surfaces of a failed high-strength steel coil spring. a.) Complete component from which failure surface specimens were extracted. b,d) Macrographs of both sides of the failure surface. c,e.) Macrographs with specular enhancement. Linear marks on both fracture surfaces radiate out from the fracture origin.

torsion fracture morphology with a helical fracture angled at roughly 45° to the wire axis [22]. The fracture surface is corroded.

Due to the heavy surface corrosion present, under normal macrographic examination (Fig. 4a&c) it is impossible to distinguish any surface markings that would help determine the failure mechanism or the direction of fracture, regardless of the incident lighting direction. Taking an RTI image series and creating a composite image with specular enhancement improves the visibility of topographical features of the fracture surface (Fig. 4b&d). It contains radial markings obscured by corrosion, which indicate that the coil spring was subject to fatigue crack growth originating at the surface point. Although winding marks caused by the spring's manufacturing process were observed on the sides of the coil, the initiation point did not correspond to a manufacturing mark. Instead, it coincided with a small semi-circular corrosion pit in a region where the spring's extruded polymer coating had been damaged. This mechanism of fatigue or corrosion-fatigue originating at a surface pit is a common failure mode for road vehicle suspension springs [23–26]. The corrosion on the fracture surface is believed to have occurred partly during service as the fatigue crack progressed, but chiefly after failure due to poor storage conditions of the component.

An example of how specularity-enhanced RTI composite images can be used in materials engineering is shown in Fig. 5. This shows a cylindrical uniaxial tensile test specimen of Ti-6Al-4 V titanium alloy machined from specimens of material which had been additive-manufactured using Electron-Beam Melting (EBM). It was locally exposed to an aerated solution of 3.5%wt NaCl at room temperature for 24 h and subjected to a maximum vertex potential of 6 V, causing surface corrosion. Specularity-enhanced RTI composite images show much more detail in the corroded area than it is possible to identify from single macrographs. With enhanced specularity, it is observed that the corroded area has well-defined and deeply-cut edges with an uneven interior; this is characteristic of a surface corrosion process which has advanced rapidly after breaching the material's passivation layer. This is consistent with the apparent interaction of the edges of the corroded area with the specimen's turning marks, as shown in Fig. 5g.

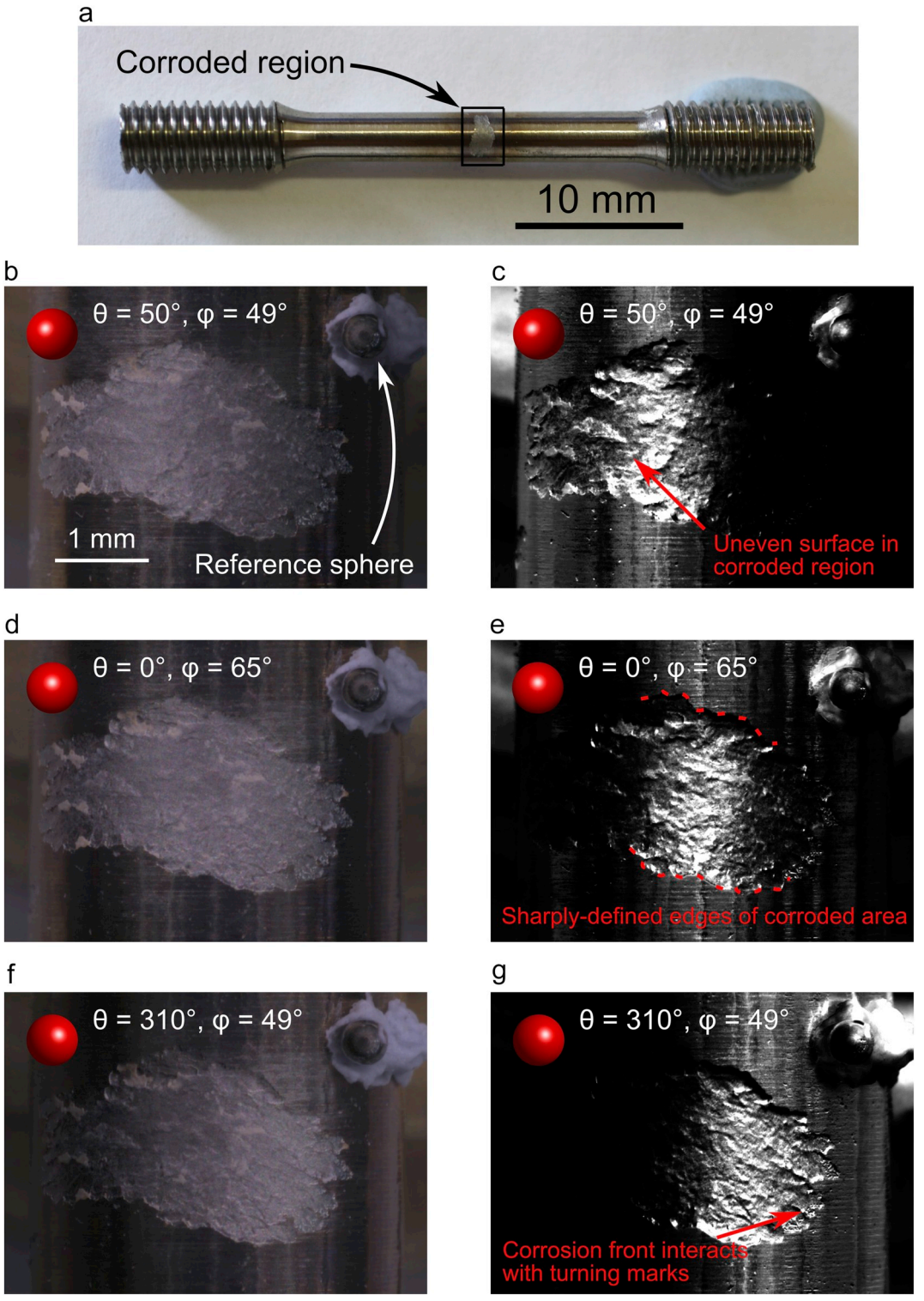

Fig. 5. Tensile test specimen of additive-manufactured titanium alloy Ti-6Al-4 V with a region of surface corrosion. a.) Overall view of the specimen showing the location of the corroded area. b,d,f.) Macrographs of the corroded curved surface with three different lighting angles. c,e,g.) Macrographs with specular enhancement at the same three lighting angles.

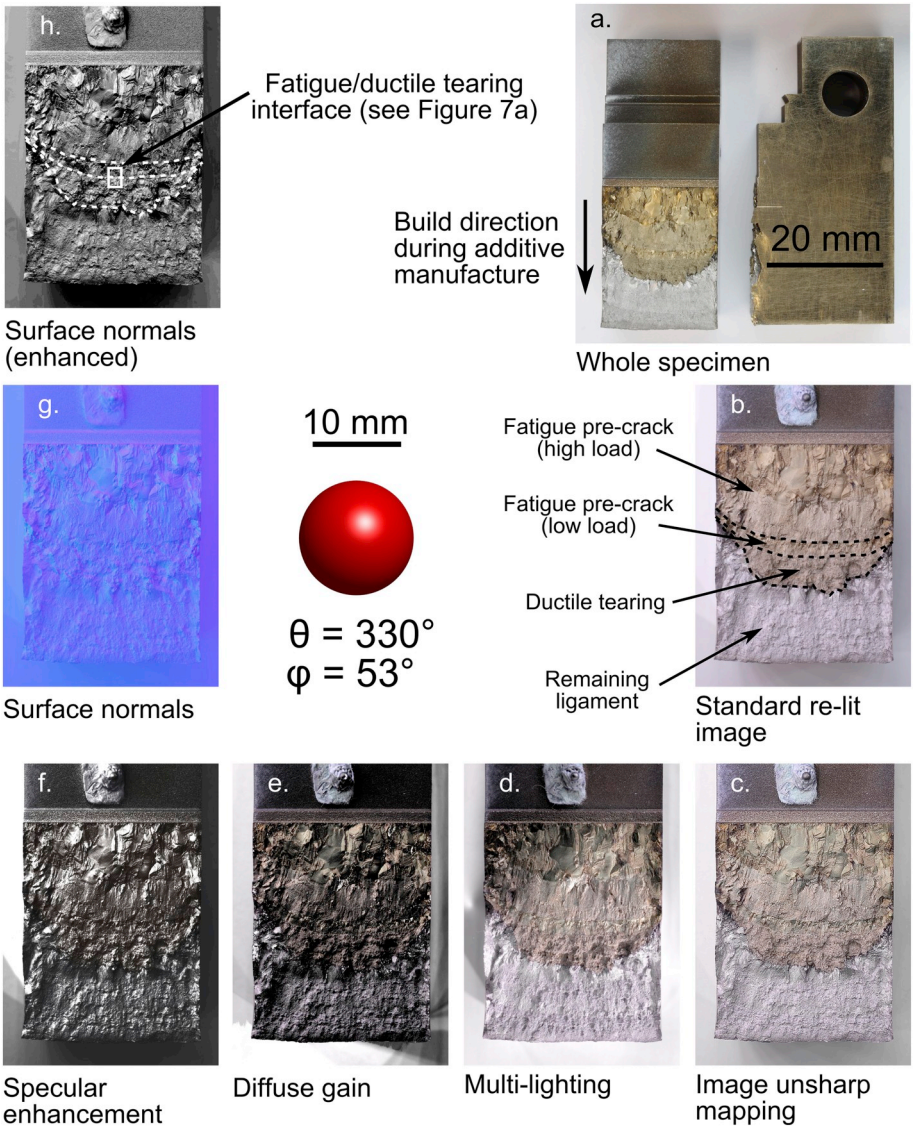

Fig. 6. a.) Failure surface of a fractured specimen of WAAM Inconel 718. b-h.) Seven examples of composite images which can be generated using RTI data, as described by Malzbender et al. [4] and Palma et al. [27].

2.3. Other visualisation methods

In addition to virtual re-lighting and specular enhancement, RTI enables other visualisation techniques which are useful for failure analysis, many of which have been implemented in RTIViewer [19,27]. A comparison of visualisation modes is shown in Fig. 6. The subject is the fracture surface of Compact (Tension) fracture test specimen of additive-manufactured nickel superalloy Inconel 718. The material was deposited using the Wire + Arc Additive Manufacturing (WAAM) process before being subjected to post-deposition heat treatment, after which the specimen was machined, fatigue pre-cracked and then loaded. Analysis by Electron Back-Scatter Diffraction (EBSD) and Neutron Diffraction (ND) demonstrated that the material was coarse-grained, with a characteristic grain diameter of approximately 0.5 mm. The specimen was also heat-tinted before being broken open: the free surface at the time of heat-tinting has a bronze colour due to oxidation, visible in Fig. 6.

As in the previous examples, the composite image with specular enhancement (Fig. 6f) gives an improved view of the specimen's surface morphology. A visualisation of the surface normals data estimated using photometric stereo also gives a good view of the surface relief, particularly when converted to greyscale and contrast-enhanced (Fig. 6 h). The specimen has a large-faceted surface in the area of pre-test fatigue crack growth and a more complex, torn surface in the region created by continuous loading. After heat-tinting, the interface between these two can be difficult to distinguish under normal lighting, but is easier to see with the benefit of interactive virtual re-lighting (Fig. 6b) or a multi-light composite image (Fig. 6d). These techniques were used to define regions of interest for subsequent SEM imaging (Fig. 7). Unsharp mapping and multi-lighting (Fig. 6c&d) make it easier to distinguish feature

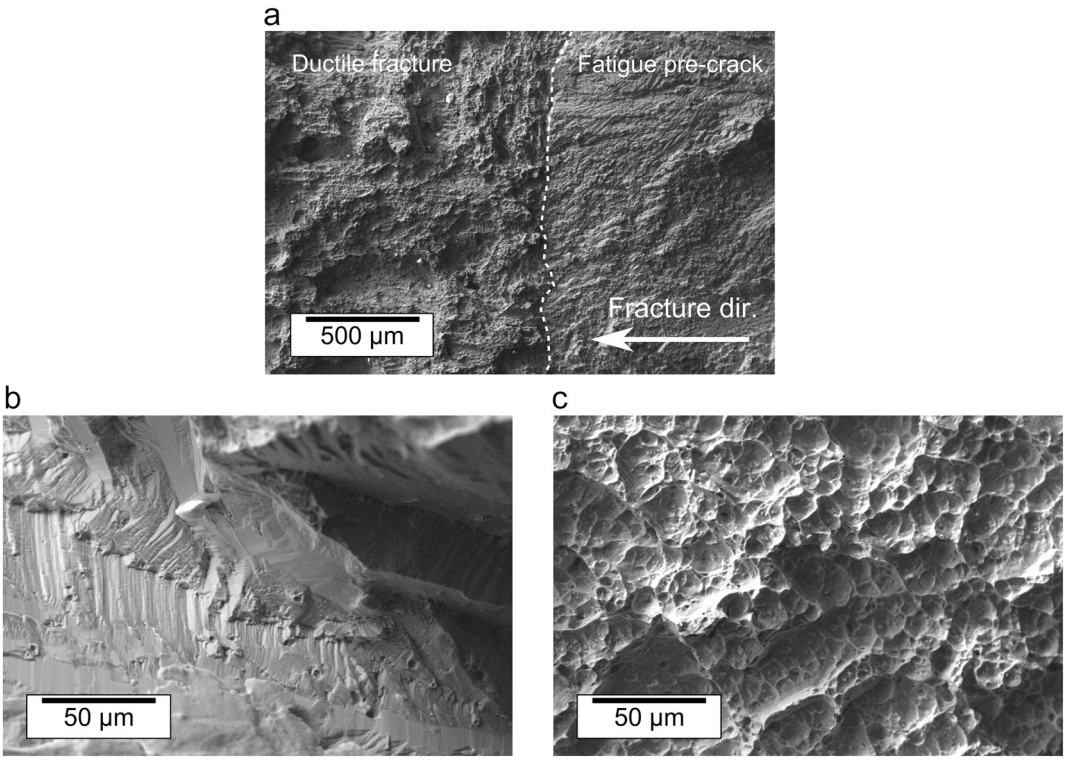

Fig. 7. SEM fractographs from the fracture surface shown in Fig. 6. a.) Interface between fatigue pre-crack and ductile fracture, b.) fatigued surface, c.) ductile fracture surface.

edges while preserving differences in surface colour. Parallel linear structures on the fatigued part of the surface are visible in the standard re-lit image but are highlighted by unsharp mapping (Fig. 6b and c, respectively).

2.4. Photometric stereo

RTI can provide an approximation of the specimen's surface height variation. To achieve this, the surface's local normal vector (see Fig. 8) at each pixel is first estimated by finding the unit vector which, when used in the fitted texture map, maximises the pixel's luminance [4]. Fig. 6 g shows surface normals estimated in this way: the image RGB values are proportional to the x,y,z components of the unit normal vector. The normal vectors are then integrated to give the point-to-point variation in surface height. This can be done using a regularisation scheme such as the one proposed by Frankot and Chellappa [28].

Several features of the RTI process can cause inaccuracy in the reconstructed height map [7]. For example, RTI lighting models typically assume that in each image the subject is lit with uniform intensity from a remote source whereas in reality each light source is a finite distance from the subject [29]. Non-Lambertian scattering from the specimen surface as well as surface self-shadowing can introduce further errors in the surface normal vector estimation. Most significantly, the height information provided by RTI is particularly subject to low-frequency errors which are inevitably introduced during the integration of the surface normals [28,30]. MacDonald and co-workers have used frequency-domain synthesis of RTI height data with height information from independent measurements to improve the accuracy of the result [7,31]. However, this requires an additional measurement of the specimen using a height gauge or Coordinate-Measuring Machine (CMM).

In this study, each subject's surface normals were extracted from an HSH texture map fitted using RTIBuilder. In the HSH model, the luminance at a given position is given by:

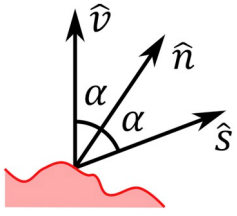

Fig. 8. Specular reflection from a surface. The surface's normal vector ($\hat{n}$) bisects the specular vector ($\hat{s}$) and the direction of the viewer ($\hat{v}$).

$$I = H_l^m(\theta, \varphi) \tag{2}$$

where I is the luminance, H_l^m is a HSH function described in detail by Gautron et al., θ is the light source azimuth and φ is the light source elevation [5,7,8]. The specular vector can be determined as the lighting position where the observed luminance is maximised:

$$[\theta_S, \varphi_S] = \underset{\theta,\varphi}{\operatorname{argmax}}\, H_l^m(\theta, \varphi) \tag{3}$$

where θ_S and φ_S are the azimuth and elevation of the specular vector, respectively. If the viewer is located directly above the specimen, then:

$$\theta_N = \frac{\theta_S}{2} \; and \; \varphi_N = \varphi_S \tag{4}$$

so the surface's normal vector is:

$$\hat{n} = [\cos\varphi_N \sin\theta_N, \sin\varphi_N \sin\theta_N, \cos\theta_N] \tag{5}$$

Surface normals for each pixel in the image, estimated using RTIBuilder, were used to form an integrable surface using the method of Frankot & Chellappa [28]. Custom code written in MATLAB (The Mathworks inc., Natick, USA) [32] was used to import, integrate and display the spatial data. In the example below, registration with optical CMM data was performed using the Iterative Closest Point algorithm [33].

An example of a 3D surface measurement using RTI is shown in Fig. 9. The subject is a fracture toughness test specimen of a ferritic pressure vessel steel which was loaded continuously until failure occurred by ductile tearing. This specimen was chosen because the fracture surface is extremely rough and uneven due the tearing mechanism of material failure, as well as being visibly warped by plastic deformation, making it challenging to measure. Focus-Variation Microscopy (FVM) surface scans were performed using an InfiniteFocus G4 optical CMM (Alicona Imaging GmbH, Graz, Austria). The accuracy of surface height information from this FVM measurement was estimated to be 0.80 µm so the specimen surface model shown in Fig. 9c was considered 'exact' for comparison purposes. The corresponding surface model from RTI photometric stereo is shown in Fig. 9d; note that both techniques also provide surface colour information. Fig. 9e&f shows a comparison of height information from FVM and RTI. The RTI height map is visibly domed towards the centre of the specimen. After registration of the point clouds was performed the root mean squared error in Euclidean distance between them was 0.89 mm and height discrepancies of > 1.5 mm occurred on the fracture surface. The RTI photometric stereo surface model (Fig. 9d) allows a basic, qualitative appreciation of the form of the real specimen but is clearly subject to significant distortion.

3. Discussion

3.1. Practical observations

In practical terms, this study has demonstrated that macro-RTI suitable for use in engineering failure analysis can be performed simply and at remarkably low cost. Excluding the laptop computer, but including the camera and optics, the total cost of materials for the RTI macro-photography setup shown in Fig. 2 was less than £900. Similarly to Cosentino [34], we found that common low-cost macrophotography techniques such as the combination of a 50 mm macro lens with an extension tube, or a 24 mm lens with a reversing ring, produced images which were adequately sharp for interpretation of the failure surface. When capturing images for RTI of small specimens, an adequately large stand-off distance between the lens and subject was needed to prevent shadowing at higher lighting elevations. Although no physical anti-vibration measures were required, SLR mirror lock-up was used to prevent any vibrations caused by the camera itself. With the lighting array and control system described above, the imaging process was straightforward and fast. Imaging took < 3 mins per image set for all of the examples shown here, some of which used very long exposures.

RTI data captured using the setup described here would be suitable for archival use [13]. A typical uncompressed project for a single capture, consisting of 48 .jpeg images at 24 megapixels, a finished .rti or .ptm file produced by RTIBuilder and other smaller files (such as a data files defining incident lighting vectors) was typically 700 MB in size.

3.2. Capabilities and limitations of RTI

Reflectance Transformation Imaging offers several useful capabilities for the failure analyst. Its chief advantage over normal macrophotography is that it allows users to distinguish surface relief features on complex surfaces, i.e. those that are rough and/or have a varying specularity and colour, much more reliably. Such complex surfaces are common in failure analysis and materials engineering, eg. fracture faces and corroded areas. RTI can firstly give the analyst an improved qualitative appreciation of surface features using techniques such as raked lighting and specular highlighting.

In archaeology, art history and preservation studies, the qualitative "feel" of surface features on an artefact often informs how the artefact is interpreted by a researcher. By contrast, in engineering and the physical sciences there can be a reluctance to use non-quantitative methods of analysis. We propose that the greater uptake of RTI in cultural heritage applications as opposed to engineering is due both to this difference in outlook and to a greater range of potential applications (eg. palaeography and brushwork analysis). However, in material and component failure analysis expert qualitative interpretation of surfaces is an essential tool and an

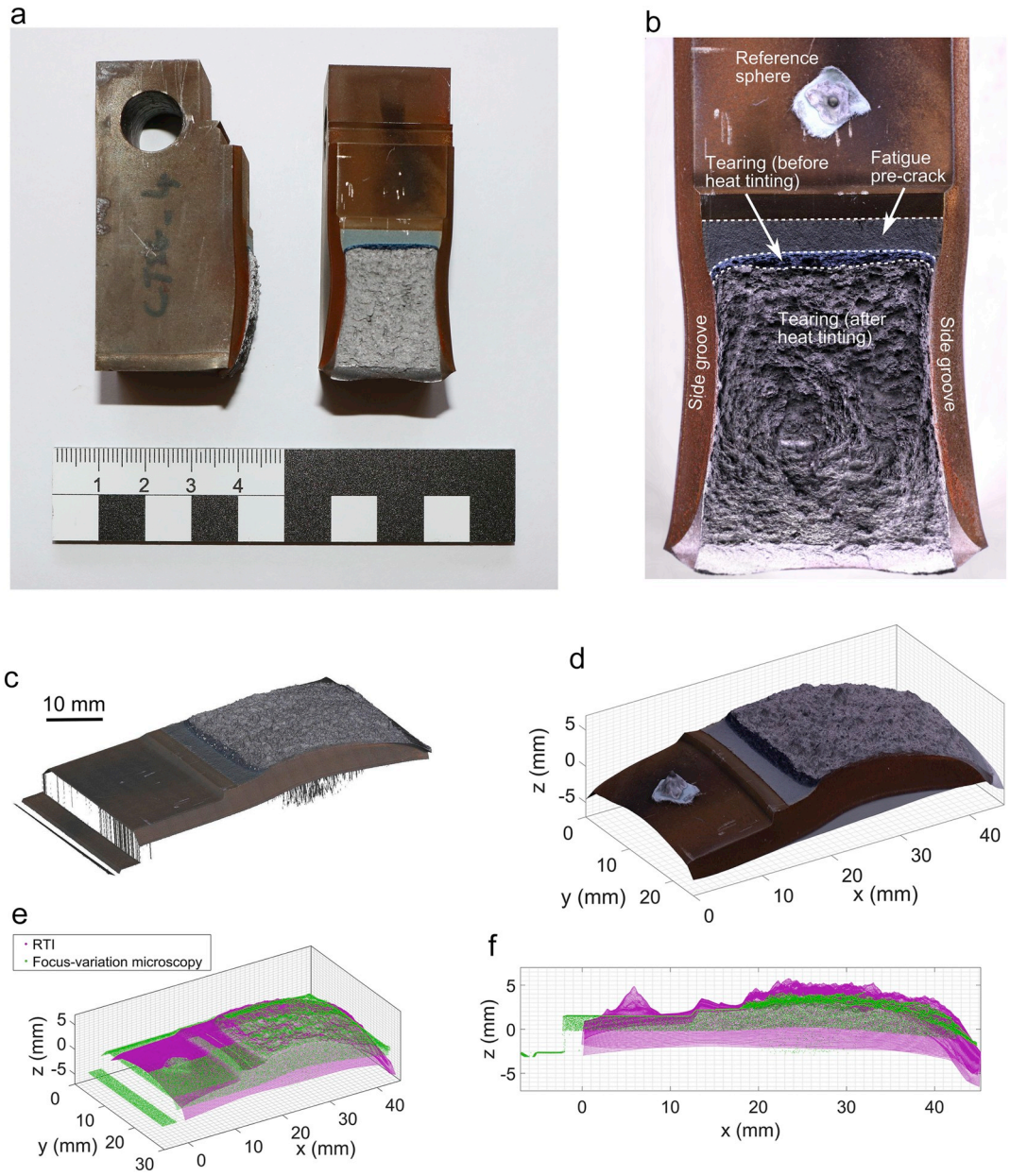

Fig. 9. a.) Failed Compact (Tension) specimen of a ductile C–Mn steel (BS 1501–224 28B). b.) RTI composite image of the fracture surface with PTM multi-lighting feature enhancement. c.) Fracture surface measured using focus-variation microscopy. Both height and colour information is recovered using this technique. d.) Fracture surface measured using RTI. e,f.) Comparison of Focus-variation microscopy and RTI surfaces – both data sets have been down-sampled for clarity.

accepted practice. A similar situation exists in both forensic pathology and criminal forensics, were RTI has also started to find application [35,36]. Therefore, failure analysis is the area of engineering most likely to benefit from the application of RTI as well as being a field where the technique is likely to find acceptance.

RTI can be used as a digitisation tool to preserve virtual specimens for future study [13]. This is useful in the context of engineering, as failed components are often difficult to store in a way that preserves their essential features. For example, they may require careful handling to prevent damage to a fracture surface or may require dessicator storage to reduce corrosion. RTI can preserve the intuitive 'feel' of a failure surface prior to disposal of a large specimen or extraction of smaller samples for further analysis. Unlike stereo-pair images, RTI data can be viewed without special-purpose hardware using a normal computer or tablet.

In addition to 2D visualisation, the RTI technique can be used to provide rudimentary 3D height mapping capability via photometric stereo. However, as shown by MacDonald and co-workers [7,12,30,31,37] and demonstrated in Fig. 9 above, RTI photometric stereo does not provide accurate height data on its own. It is subject to long-range distortions and does not approach the

accuracy of an optical CMM using Focus-Variation Microscopy (FVM). In addition to FVM, many other small-scale coordinate measurement techniques such as Confocal Laser Scanning Microscopy (CLSM), Coherence Scanning Interferometry (CSI), laser line scanning and contact profilometry are available, and all would provide more accurate height information for specimens relevant to engineering failure analysis. Although RTI photometric stereo should not be used when accurate shape reconstruction is needed, in the context of failure analysis it may be useful for qualitative visualisation of shape.

RTI does not provide the high 2D spatial resolution that can be achieved using optical microscopy or SEM. It also does not provide the accurate 3D topology measurements that are possible using FVM, CSI, CLSM or contact profilometry. Instead, RTI is a purely photometric approach: a powerful and effective improvement to macro-photographic examination. It complements rather than replaces geometric techniques such as photogrammetry [38]. RTI greatly aids the manual identification of features on complex surfaces and so is particularly well-suited to interpreting material and component failures.

4. Conclusions

Reflectance Transformation Imaging can be used to characterise the visual appearance of surfaces for engineering failure analysis. Macro-photography RTI can distinguish failure surface features in a size range of roughly 10 μm to 10 mm. The technique provides much more information about the failure surface's shape and its interactions with incident light than a normal macro-photograph. In this article we have presented several examples which demonstrate that RTI composite images can allow a specimen's surface topology to be distinguished under very adverse conditions. Since the failure surfaces of real components are almost always complex (e.g. simultaneously coloured, rough and non-uniformly reflective), we have found that RTI is extremely useful in the context of material and component failure analysis.

RTI can also be used for photometric stereo, giving an ad hoc 3D reconstruction of surface relief. However, currently this does not approach the accuracy of competing methods for 3D surface scanning. Although RTI is currently limited to low-magnification visible-light examination, there appear to be no fundamental barriers to its use at much higher optical magnifications.

Acknowledgements

The authors are grateful to Dr. N. O. Larrosa, Dr. R. Leiva-Garcia and Dr. K. L. A. Hore for providing specimens. Funding for this study was provided by the UK Engineering and Physical Sciences Research Council under grant no. EP/M019446/1 and by the University of Bristol.

Declaration of interest

We declare that there are no conflicts of interest affecting this work.

Data access statement

Supplementary images and texture maps for all of the examples given in this article can be downloaded from: https://doi.org/10.5523/bris.2g3lyqy6ywy1j1z3owrijsom0i

References

[1] D.A. Ryder, T.J. Davies, I. Brough, F.R. Hutchings, General practice in failure analysis, in: G.W. Powell, S.E. Mahmoud (Eds.), ASM Metals Handbook, Failure Analysis and Prevention, vol. 11, ASM International, 1986, pp. 15–46.
[2] C.R. Brooks, A. Choudhury, Failure Analysis of Engineering Materials, McGraw Hill, 2002.
[3] Ø. Hammer, S. Bengtson, T. Malzbender, D. Gelb, Imaging fossils using reflectance transformation and interactive manipulation of virtual light sources, Palaeontol. Electron. 5 (4) (2002) 1–9.
[4] T. Malzbender, D. Gelb, H. Wolters, Polynomial texture maps, SIGGRAPH '01 Proceedings of the 28th annual conference on Computer graphics and interactive techniques, 2001, pp. 519–528.
[5] P. Gautron, J. Krivanek, S. Pattanaik, K. Bouatouch, A novel hemispherical basis for accurate and efficient rendering, Eurographics Symposium on Rendering, 2004, pp. 321–330.
[6] O. Wang, P. Gunawardane, S. Scher, J. Davis, Material classification using BRDF slices, 2009 IEEE Conference on Computer Vision and Pattern Recognition, 2009, pp. 2805–2811.
[7] L.W. MacDonald, Representation of cultural objects by image sets with directional illumination, CCIW 2015: Computational Color Imaging, 2015, pp. 43–56.
[8] G. Pitard, G.L. Goïc, A. Mansouri, H. Favrelière, S.-F. Desage, S. Samper, M. Pillet, Discrete Modal Decomposition: a new approach for the reflectance modeling and rendering of real surfaces, Mach. Vis. Appl. 28 (2017) 607–621.
[9] T. Malzbender, B. Wilburna, D. Gelb, B. Ambrisco, Surface enhancement using real-time photometric stereo and reflectance transformation, Proceedings of the 17th Eurographics Symposium on Rendering, 2006.
[10] S.M. Duffy, Multi-Light Imaging for Heritage Applications, English Heritage, 2013.
[11] G. Earl, K. Martinez, T. Malzbender, Archaeological applications of polynomial texture mapping: analysis, conservation and representation, J. Archaeol. Sci. 37 (2010) 2040–2050.
[12] L. MacDonald, M.F. Guerra, R. Pillay, M. Hess, S. Quirke, S. Robson, A.H. Ahmadabadian, Practice-based comparison of imaging methods for visualization of toolmarks on an Egyptian scarab, 6th International Conference on Image and Signal Processing, 2014, pp. 239–246.
[13] M. Mudge, T. Malzbender, A. Chalmers, R. Scopigno, J. Davis, O. Wang, P. Gunawardane, M. Ashley, M. Doerr, A. Proenca, J. Barbosa, Image-based empirical information acquisition, scientific reliability, and long-term digital preservation for the natural sciences and cultural heritage, Proceedings of Eurographics 2008, 2008.
[14] H. Mytum, J.R. Peterson, The application of Reflectance Transformation Imaging (RTI) in historical archaeology, Hist. Archaeol. 52 (2) (2018) 489–503.

[15] G. Pitard, Métrologie et modélisation de l'aspect pour l'inspection qualité des surfaces (in French), Université Grenoble Alpes, 2016.
[16] G. Pitard, G.L. Goic, A. Mansouri, H. Favrelere, M. Pillet, S. George, J.Y. Hardeburg, Reflectance-based surface saliency, Proceedings of the 24th IEEE International Conference on Image Processing, 2017.
[17] P. Gunawardane, O. Wang, S. Scher, I. Rickards, J. Davis, T. Malzbender, Optimized image sampling for view and light interpolation, The 10th International Symposium on Virtual Reality, Archaeology and Cultural Heritage VAST, 2009.
[18] "RTIBuilder Version 2.0.2", Cultural Heritage Imaging, (2011).
[19] RTIViewer Version 1.1, Cultural Heritage Imaging, (2013).
[20] T.M. Clarke, Photography of fractured parts and fracture surfaces, ASM Metals Handbook Volume 12: Fractography, ASM International, 1987, pp. 150–176.
[21] B.T. Phong, Illumination for computer generated pictures, Commun. ACM 18 (6) (1975) 311–317.
[22] J.H. Maker, Failures of springs, in: G.W. Powell, S.E. Mahmoud (Eds.), ASM Metals Handbook, Failure Analysis and Prevention, vol. 11, ASM International, 1986, pp. 550–562.
[23] Y. Ashida, Y. Daigo, K. Sugahara, An industrial perspective on environmentally assisted cracking of some commercially used carbon steels and corrosion-resistant alloys, *JOM*, J. Minerals, Metals Mater. Soc. 69 (8) (2017) 1381–1388.
[24] L. Kosec, A. Nagode, G. Kosec, D. Kovacevic, B. Karpe, B. Zorc, B. Kosec, Failure analysis of a motor-car coil spring, Case Studies Engineer. Failure Anal. 4 (2015) 100–103.
[25] G. Vukelic, M. Brcic, Failure analysis of a motor vehicle coil spring, Procedia Struct. Integr. 2 (2016) 2944–2950.
[26] Y. Zhu, Y. Wang, Y. Huang, Failure analysis of a helical compression spring for a heavy vehicle's suspension system, Case Studies Engineer. Failure Anal. 2 (2) (2014) 169–173.
[27] G. Palma, M. Corsini, P. Cignoni, R. Scopigno, M. Mudge, Dynamic shading enhancement for reflectance transformation imaging, ACM J. Comp. Cultural Heritage 3 (2) (2010) 6.1–6.20.
[28] R.T. Frankot, R. Chellappa, A method for enforcing integrability in shape from shading algorithms, IEEE Trans. Pattern Anal. Mach. Intell. 10 (4) (1988) 439–451.
[29] X. Huang, M. Walton, G. Bearman, O. Cossairt, Near light correction for image relighting and 3D shape recovery, Proceedings of the 2015 Digital Heritage International Congress, vol. 1, 2015, pp. 215–222.
[30] L.W. MacDonald, Realistic Visualisation of Cultural Heritage Objects, University College London, 2015.
[31] L. MacDonald, V.M. de Almeida, M. Hess, Three-dimensional reconstruction of Roman coins from photometric image sets, J. Electronic Imaging 26 (1) (2017) 011017.
[32] MATLAB®, version 9.0.0.370719 (R2016a). Natick, USA: The Mathworks Inc.
[33] P.J. Besl, N.D. McKay, A method for registration of 3-D shapes, IEEE Trans. Pattern Anal. Mach. Intell. 14 (2) (1992) 239–256.
[34] A. Cosentino, Macro photography for reflectance transformation imaging: a practical guide to the highlights method, e-Conserv. J. 1 (2013) 70–85.
[35] S. Clarke, A.M. Christensen, Reflectance Transformation Imaging (RTI) of saw marks on bones, J. Forensic Radiol.Imaging 7 (2016) 33–37.
[36] J.S. Hamiel, J.S. Yoshida, Evaluation and Application of Polynomial Texture Mapping (PTM) in the Area of Shoe/Tire Impression Evidence, National Institute of Justice, 2012 2004-IJ-CX-K008.
[37] L. MacDonald, I. Toschi, E. Nocerino, M. Hess, F. Remondino, S. Robson, Accuracy of 3D reconstruction in an illumination dome, The International Archives of the Photogrammetry, Remote Sensing and Spatial Information Sciences: Volume XLI-B5, XXIII ISPRS Congress, 2016, pp. 69–76.
[38] S.T. Porter, N. Huber, C. Hoyer, H. Floss, Portable and low-cost solutions to the imaging of Paleolithic art objects: a comparison of photogrammetry and reflectance transformation imaging, J. Archaeol. Sci. Rep. 10 (2016) 859–863.